Modelling of a Plasmonic Biosensor Based on a Graphene Nanoribbon Superlattice

*André Souto, Diogo Cunha, Mikhail I. Vasilevskiy**

Optional dedication here. If no dedication is required, please leave blank

André Souto
Centro de Física das Universidades do Minho e do Porto, Universidade do Minho, Braga 4710-057, Portugal
Email Address: andresouto995@hotmail.com
Diogo Cunha
Centro de Física das Universidades do Minho e do Porto, Universidade do Minho, Braga 4710-057, Portugal
Mikhail I. Vasilevskiy
Centro de Física das Universidades do Minho e do Porto and Departamento de Física, Universidade do Minho, Braga 4710-057, Portugal
International Iberian Nanotechnology Laboratory, Av. Mestre José Veiga s/n,
Braga 4715-330, Portugal

Keywords: *graphene, superlattice, nanoribbons, biosensor, plasmonics, biomolecules*

We present a semi-analytical theoretical model, which describes the operation of a selective molecular sensor [1] employing a double resonance between a dipole-active molecular vibration mode, tunable surface plasmons in a periodic structure of graphene nanoribbons (NRs), and the incident light, in the THz-to-IR range, used for testing. The model is based on the solution of Maxwell's equations for the NR structure deposited on a dielectric substrate, using the electromagnetic Green's function, and is extended to the case of an additional (buffer) layer present between the NRs and the substrate. Both the graphene NRs and the layer of adsorbed molecules are considered as two-dimensional, since their thicknesses are very small in comparison with the wavelength of the incident light. The model is applied to different molecular systems, the protein studied in Ref. [1], for which an excellent agreement with experimental data is obtained, and an organometallic molecule $Cd(CH_3)_2$. Two different assumptions concerning the way of sticking of the analyte molecules to the sensor's surface are considered and the limitations of this sensing principles are discussed.

1 Introduction

Graphene, a 2D crystal made up of carbon atoms arranged in a honeycomb lattice, is a very versatile material with a plethora of already demonstrated and potential applications. [2] Its unique conical band structure near the Dirac point results in a set of exceptional electronic and optical properties, which are explored, in particular, in the area of Plasmonics. [3–5]

Graphene plasmons, propagating oscillations of free electrons confined to one atomic plane, which occur in the THz-to-mid-infrared spectral range, were demonstrated experimentally for the first time in 2012. [6,7] Since then, a lot of experimental and theoretical research on their properties and applications has been carried out, reviewed in Refs. [4,5,8–10] Similar to noble metals, plasmons in graphene also exhibit strong electromagnetic (EM) confinement and therefore high near–field intensity. [11,12] This is particularly important in the region extending from the THz to the mid-IR, because in this spectral range noble metal plasmons are poorly confined and lossy. Therefore, graphene emerges as a technological material able to perform in a spectral range where noble metals fail.

As known, surface plasmons cannot be launched directly by a propagating electromagnetic (EM) wave because of the wavevector mismatch. [13] They are coupled to an evanescent EM wave and form surface plasmon-polaritons (SPPs). There are several methods for achieving the wavector matching and exciting SPPs in graphene by incident light, [9] of which probably the most popular one is patterning it into a periodic array of nanoribbons. [1,14–17] The spatial period of the array determines the frequencies of the SPPs which, additionally, can be tuned by applying a gate voltage to the graphene nanoribbons (another advantage of graphene compared to noble metals). [6,14,18,19]

One important application of surface plasmonsis in the area biomolecular and environment sensing. The most paradigmatic sensing principle is based on the surface plasmon resonance (SPR) and such sensors

have been commercialized by several companies since the 1990-th. [20] The resonance between the incident light of a certain wavelength and the SPPs, mediated by a prism in the Kretschmann configuration or by a grating, occurs at a well defined angle of incidence, which is very sensitive to the dielectric properties of the environment of the plasmonic surface. [13,20] Initial proposals of incorporation of graphene into sensors based on this principle were limited to to covering the plasmonic (metallic) film by graphene layers for improving the adsorption of analyte molecules. [8] Later, the idea of using graphene for the electrical control of the SPPs induced metallic nanostructures has also been explored. [10,21–23] Despite their high sensitivity, a shortcoming of conventional SPR-based sensors is the lack of selectivity. The sensing can be made species-selective if the resonance is pushed to longer wavelengths. Indeed, most of the molecules have a clear and specific spectroscopic signature in the THz and mid-IR, which can be identified by IR absorption spectroscopy. [24] This is a powerful technique since it can be used to extract useful information without requiring any sort of labeling or destruction of the samples. However, the vibrational signals of biomolecules are rather weak and hard to isolate in the IR absorption spectra. This limitation can be eliminated or at least mitigated by taking advantage of the strong optical near fields characteristic of the SPR. Reaching the FIR spectral range is not possible with flat metal surfaces but may be achieved with specially designed nanoantennas [25,26] or, for some molecules, with spoof plasmons. [27] However, these suffer from all the previously mentioned weaknesses, the poor confinement in this spectral range and limited tunability. [10,28]

Thankfully, graphene is a viable alternative to these systems, especially when arranged in a periodic sequence of nanoribbons (NRs), a superlattice (SL), which allow for the direct excitation of the SPPs. Owing to the intense EM fields created by the SPPs, the specific molecular spectroscopic resonances are boosted to become clearly visible in the excitation spectrum of the array of nanoribbons. Therefore, this method emerges as a promising strategy for the creation of sensors using this physical principle, in some sense similar to the surface-enhanced Raman spectroscopy (SERS). [29], and the protein sensing has been achieved by detecting narrow dips corresponding to molecular vibration bands. [1,30]

In this work, we will present a semi-analytical model of a graphene NR SL sensor of the type devised in Ref. [1] The optical properties of a graphene NR SL on a dielectric substrate have been investigated theoretically before [9,16] but here we shall use a different (namely, EM Green's function) approach to derive the EM fields and extend it to a structure with an additional dielectric layer (shown in the inset of Figure 1). The graphene is described by its 2D optical conductivity [5], $\sigma_G(\omega)$, and the molecules are added to the system by simply adding their conductivity to $\sigma_G(\omega)$. We shall present calculated results that reproduce very well the experimental data [1] and allow for optimization of graphene nanoribbon structures in order to detect another type of molecular species, an organometallic compound $Cd(CH_3)_2$.

2 Graphene NR superlattice

2.1 Model and approach

We begin by deriving the scattering of a plane EM wave while traversing a 2D interface with a periodically modulated conductivity. For a transverse magnetic (TM) wave of a frequency ω, with the components $\mathbf{B} = (0, B_y, 0)$ and $\mathbf{E} = (E_x, 0, E_z)$ (the coordinate frame is shown in 1)), and for an interface with the conductivity $\sigma(x, \omega)$ that depends on the position x, the magnetic field derivative obeys the following integral equation that follows from the discontinuity condition: [9]

$$2B_0 e^{ik_x x} + \frac{i}{2\epsilon_1}\int_{-\infty}^{\infty} dx' g(|x-x'|)\frac{\partial B_y(x)}{\partial z}\bigg|_{z=0^+} = -i\frac{4\pi\sigma(x,\omega)}{\epsilon_1\omega}\frac{\partial B_y(x)}{\partial z}\bigg|_{z=0^+}, \tag{1}$$

where $g(|x-x'|)$ is the Green's function given by

$$g(|x-x'|) = \epsilon_1 H_0^{(1)}(k_1|x-x'|) + \epsilon_2 H_0^{(1)}\left(\sqrt{k_2|x-x'|}\right), \tag{2}$$

where $H_0^{(1)}$ is the Hankel function of the first kind, $k_i = \sqrt{\epsilon_i}\omega/c$ and ϵ_i ($i = 1, 2$) is the dielectric permittivity of each medium (see Sec. 7 of Ref. [9] for details of the derivation).

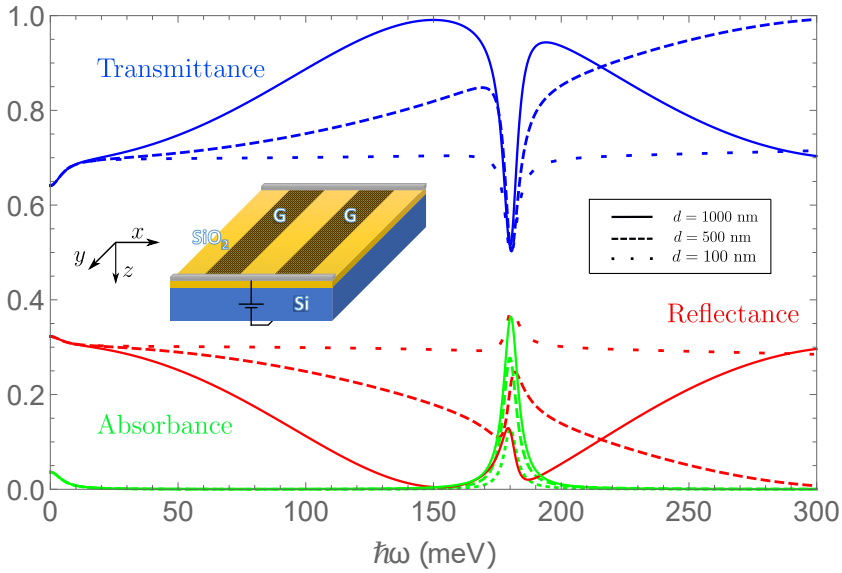

Figure 1: Normal incidence optical spectra of the structure shown in the inset, calculated for different values of the SiO_2 layer thickness (d), with the following parameters: $\epsilon_1 = 1$, $\epsilon_2 = 3.9$, $\epsilon_2 = 11.8$, $E_F = 0.35$ eV, $\Gamma = 5$ meV, $D = 40$ nm and $d_1 = d_2 = D/2$. Notice the absorbance peak corresponding to the 1-st plasmonic resonance of the NR SL.

Let us define a function, $f(x)$, proportional to the magnetic field derivative, i.e. the transverse electric field at the interface. Since $\sigma(x,\omega)$ is a periodic function in the case we are interested in here, we can expand $f(x)$ in a Fourier series,

$$f(x) = \frac{1}{\epsilon_1 B_0}\frac{\partial B_y(x)}{\partial z}\bigg|_{z=0^+} = e^{ik_x x}\sum_{n=-\infty}^{+\infty} a_n e^{i\frac{2\pi n}{D}} \ , \tag{3}$$

where k_x is the in-plane component of the wavevector and D is the SL period. Multiplying Equation (1) by $\exp(-i2\pi m/D)$ (m is an integer) and integrating over the SL period, we arrive at the following system of linear equations for the coefficients a_n:

$$2i\delta_{m,0} = \frac{4\pi}{\omega}\sum_{n=-\infty}^{+\infty} a_n\sigma_{nm}(\omega) + a_m\left(\frac{\epsilon_1}{q_{1m}} + \frac{\epsilon_2}{q_{2m}}\right) \ . \tag{4}$$

Here,

$$q_{in} = \sqrt{\epsilon_i\frac{\omega^2}{c^2} - \left(k_x + \frac{2\pi}{D}n\right)^2} \tag{5}$$

k_x is the $x-$component of the wavevector,

$$\sigma_{nm}(\omega) = \begin{cases} \frac{\sigma_1(\omega)d_1+\sigma_2(\omega)d_2}{D} \equiv \bar{\sigma} & n = m \\ \frac{\sigma_2(\omega)-\sigma_1(\omega)}{2\pi i(n-m)}\left(1 - e^{\frac{2\pi i d_1}{D}(n-m)}\right) & n \neq m \end{cases} \ , \tag{6}$$

and d_1 and d_2 are the widths of the NRs and the gaps between them, respectively. Equations (4) yield the coefficients a_n, which determine the scattered EM fields in the upper and lower half-spaces.
The magnetic field in the upper half-space is the sum of the scattered, reflected and incident fields, which are written as follows: [9]

$$B_y^{\text{scat}}(x, z<0) = i\epsilon_1 B_0 e^{ik_x x}\sum_{n=-\infty}^{+\infty}\frac{a_n}{q_{1n}}e^{i\left(\frac{2\pi i}{D}nx - q_{1n}z\right)} \ ; \tag{7}$$

$$B_y^{\text{ref}}(x, z<0) = B_0 e^{ik_x x - ik_{1z}z} \ ; \tag{8}$$

$$B_y^{\text{inc}}(x, z<0) = B_0 e^{ik_x x + ik_{1z}z} \ , \tag{9}$$

which leads to

$$B_y(x, z < 0) = 2B_0 \cos(k_{1z} z) + i\epsilon_1 B_0 e^{ik_x x} \sum_{n=-\infty}^{\infty} \frac{a_n}{q_{1n}} e^{i\left(\frac{2\pi n}{D} x - q_{1n} z\right)} \ . \tag{10}$$

The x component of the electric field can be expressed through Maxwell's equation in the following way:

$$E_x(x, z < 0) = -i\frac{c}{\epsilon_1 \omega} \frac{\partial B_y(x, z < 0)}{\partial z} \tag{11}$$

$$= 2iB_0 \frac{ck_{1z}}{\epsilon_1 \omega} \sin(k_{1z} z) - iB_0 \frac{c}{\omega} e^{ik_x x} \sum_{n=-\infty}^{\infty} \frac{a_n}{q_{1n}} e^{i\left(\frac{2\pi n}{D} x - q_{1n} z\right)} \ . \tag{12}$$

In the lower half-space, we have only the transmitted (scattered) wave:

$$B_y^{\text{trans}}(x, z > 0) = -i\epsilon_2 B_0 e^{ik_x x} \sum_{n=-\infty}^{+\infty} \frac{a_n e^{\frac{2\pi i}{D} nx}}{q_{2n}} e^{iq_{2n} z} \ ; \tag{13}$$

$$E_x^{\text{trans}}(x, z > 0) = -i\frac{c}{\epsilon_2 \omega} \frac{\partial B_y(x, z > 0)}{\partial z} \ . \tag{14}$$

Different terms in the above equations represent the different orders of scattering with respect to the SL period. Only those that correspond to *real* values of the $z-$component of the wavevector, q_{in}, can be observed in the far field. Let us assume for simplicity that only the zeroth order mode of the scattered field ($\propto a_0$) is propagating, while all higher modes are evanescent. As we shall see below, this assumption is valid for the structures considered below. Therefore, at large distances from the SL, the relative amplitudes of the propagating field are given by the following Fresnel coefficients:

$$\hat{r} = 1 + i\frac{\epsilon_1}{k_{1z}} a_0 \ , \tag{15}$$

$$\hat{t} = -i\frac{\epsilon_2}{k_{2z}} a_0 \ . \tag{16}$$

Here $k_{iz} \equiv q_{in}$. These expressions are valid for a NR SL cladded by two semi-infinite media.

2.2 Optical spectra of the full structure

Let us now generalise the model for the structure shown in the inset of Figure 1, with a SiO_2 buffer layer and a thick Si substrate. In the upper half-space we have the same fields as before. In the buffer layer, we have to take into account the primary scattered wave and the one reflected at the interface between the media 2 and 3,

$$B_y(x, 0 \le z \le d) = -i\epsilon_2 B_0 e^{ik_x x} \sum_{n=-\infty}^{\infty} \frac{e^{i\frac{2\pi n}{D} x}}{q_{2n}} \left(a_n e^{iq_{2n} z} + c_n e^{-iq_{2n} z}\right) \ ; \tag{17}$$

$$E_x(x, 0 \le z \le d) = -iB_0 \frac{c}{\omega} e^{ik_x x} \sum_{n=-\infty}^{\infty} e^{i\frac{2\pi n}{D} x} \left(a_n e^{iq_{2n} z} - c_n e^{-iq_{2n} z}\right) \ . \tag{18}$$

Finally, in the substrate we have:

$$B_y(x, z \ge d) = -i\epsilon_3 B_0 e^{ik_x x} \sum_{n=-\infty}^{\infty} \frac{e^{i\frac{2\pi n}{D} x}}{q_{3n}} e_n e^{iq_{3n} z} \ ; \tag{19}$$

$$E_x(x, z \ge d) = -iB_0 \frac{c}{\omega} e^{ik_x x} \sum_{n=-\infty}^{\infty} e_n e^{i\left(\frac{2\pi n}{D} x + q_{3n} z\right)} \ , \tag{20}$$

where b_n, c_n and e_n are some coefficients.
Now we have two sets of boundary conditions, one at $z = 0$,

$$\begin{cases} E_x^{(1)}(x, z = 0) = E_x^{(2)}(x, z = 0) \ ; & (21) \\ B_y^{(1)}(x, z = 0) - B_x^{(2)}(x, z = 0) = \dfrac{4\pi\sigma_G}{c} E_x^{(1)}(z = 0) \ , & (22) \end{cases}$$

and another at $z = d$,

$$\begin{cases} E_x^{(1)}(x, z = d) = E_x^{(2)}(z = d) \ ; & (23) \\ B_y^{(1)}(x, z = d) = B_x^{(2)}(z = d) \ . & (24) \end{cases}$$

Substituting the fields into these relations and noting that they must be fulfilled separately for each order n, after some algebra we arrive at the following system of equations for the coefficients a_n:

$$2i\delta_{m,0} = \frac{4\pi}{\omega} \sum_{n=-\infty}^{\infty} \sigma_{nm}(\omega) a_n + a_m \left(\frac{\epsilon_1}{q_{1m}} + \frac{\epsilon_2}{q_{2m}} \frac{1 + e^{2iq_{2m}d}\Delta_m^{23}}{1 - e^{2iq_{2m}d}\Delta_m^{23}} \right) \tag{25}$$

where

$$\Delta_m^{23} = \frac{\epsilon_3 q_{2n} - \epsilon_2 q_{3n}}{\epsilon_3 q_{2n} + \epsilon_2 q_{3n}} \ . \tag{26}$$

The coefficients e_n that determine the transmitted wave are related to a_n as follows:

$$e_n = a_n \frac{2\epsilon_3 q_{3n}}{(\epsilon_3 q_{2n} + \epsilon_2 q_{3n})\left(1 - e^{2iq_{2n}d}\Delta_n^{23}\right)} e^{i(q_{2n} - q_{3n})d} \ . \tag{27}$$

The Fresnel coefficients of the structure, under the same assumption that only the zeroth order wave is propagating, are given by:

$$\hat{r} = 1 + i\frac{\epsilon_1}{k_{1z}} a_0 \ , \tag{28}$$

$$\hat{t} = -i\epsilon_3 \frac{e_0}{k_{3z}} \ . \tag{29}$$

With these, we can calculate the reflectance, transmittance and absorbance spectra:

$$R = |\hat{r}|^2 \ ; \tag{30}$$

$$T = \frac{k_{3z}\epsilon_1}{k_{1z}\epsilon_3} |\hat{t}|^2 \ ; \tag{31}$$

$$A = 1 - T - R \ . \tag{32}$$

The coefficients a_0 are dependent on the conductivities, which we take here as

$$\begin{cases} \sigma_1(\omega) = \sigma_G(\omega) \\ \sigma_2(\omega) = 0 \end{cases} \ . \tag{33}$$

The conductivity of graphene is a sum of the part due to interband transitions, [5,9] $\sigma_I = \sigma_I' + i\sigma_I''$ with

$$\sigma_I' = \sigma_0 \left(1 + \frac{1}{\pi} \arctan \frac{\hbar\omega - 2E_F}{\hbar\gamma} - \frac{1}{\pi} \arctan \frac{\hbar\omega + 2E_F}{\hbar\gamma} \right) \ , \tag{34}$$

and

$$\sigma_I'' = -\sigma_0 \frac{1}{2\pi} \ln \frac{(2E_F + \hbar\omega)^2 + \hbar^2\gamma^2}{(2E_F - \hbar\omega)^2 + \hbar^2\gamma^2} \ , \tag{35}$$

and the intraband (Drude) term,

$$\sigma_G(\omega) = \frac{e^2 E_F}{\pi\hbar} \frac{1}{\Gamma - i\hbar\omega} \ . \tag{36}$$

Here $\sigma_0 = e^2/(4\hbar)$, γ and Γ are the relaxation rates (to be taken as equal), and $E_F > 0$ denotes the Fermi level position with respect to the Dirac point.
Figure 1 shows the normal incidence spectra ($k_x = 0$) for this case, with the parameters listed in the caption. As expected, they display an absorbance peak at a certain frequency, which corresponds to the plasmonic resonance. Considering these values, we check that all q_{in} with $n > 0$ are imaginary, in accordance with our assumption.
We notice that there is an increase in the transmittance and a respective decrease in the reflectance as the buffer layer becomes thicker. This is related with constructive/destructive interference due to the buffer layer. It helps to amplify the NR signal and the absorbance is considerably increased in the case of d=1000 nm.

2.3 Graphene NR superlattice as a biosensor

Now we will include a layer of adsorbed (bio-)molecules in the system. Since this layer is expected to be just a few nanometers' thick, we shall consider it as two-dimensional and describe by a 2D optical conductivity. The latter can be simply related to the molecular polarisability of the analyte molecules, $\alpha_0(\omega)$, as follows:

$$\sigma_M(\omega) = -i\omega\epsilon_1 N_M^{(2D)}\alpha_0(\omega) \ , \tag{37}$$

where $N_M^{(2D)}$ is the number of molecules per unit area.
The molecules studied by Rodrigo *et al.* [1], a recombinant protein A/G and the goat anti-mouse immunoglobulin G (IgG), have two IR-active vibrational modes wityh the frequencies $\omega_1 = 1668\text{cm}^{-1}$ and $\omega_2 = 1532\text{cm}^{-1}$ (corresponding to the amide I and amide II vibration bands). Therefore, we shall write Equation (37) in the form:

$$\sigma_M(\omega,\Theta) = -i\omega\epsilon_1\Theta\delta\sum_{i=1,2}\frac{\beta_i}{\omega_i^2-\omega^2-i\omega\gamma_i} \ , \tag{38}$$

where Θ is the dimensionless coverage (defined in such a manner that $\Theta = 1$ corresponds to a fully covered monolayer, $\Theta = 2$ corresponds to a bilayer, and so forth), δ the thickness of the molecular monolayer (so that $N_M^{(2D)}/\delta$ is the 3D density of the molecules in the adsorption layer), γ_i are the corresponding damping parameters and the amplitudes β_i can be related (through the Clausius-Mossotti relation) to the resonant frequencies, damping parameters and the oscillator strengths (S_i) of the vibrational bands in the frequency-dependent permittivity, $\epsilon_M(\omega)$:

$$\beta_i = \frac{3\gamma_i\omega_i}{4\pi}\text{Im}\left(\frac{\epsilon_M(\omega_i)-\epsilon_\infty}{\epsilon_M(\omega_i)+2\epsilon_\infty}\right) \ ; \tag{39}$$

$$\epsilon_M(\omega) = \epsilon_\infty + \frac{S_1^2}{\omega_1^2-\omega^2-i\omega\gamma_1} + \frac{S_2^2}{\omega_2^2-\omega^2-i\omega\gamma_2} \ . \tag{40}$$

The permittivity $\epsilon_M(\omega)$ of the condensed phase of the molecules was measured experimentally by Rodrigo *et al.* [1] and $\epsilon_\infty \approx 2.1$ in Equation (39) is a background dielectric constant. Details of the derivation of Equation (39) can be found in the Supplementary Information.
As already pointed out, the thickness of the molecular layer, δ, is very small, $k_{1z}\delta \ll 1$, so we can safely assume that the molecules and the graphene experience exactly the same EM field, including its propagating and evanescent components, $\mathbf{E}(x, z = 0)$. So, we should be able to model the biosensor by simply adding the optical conductivity of the molecules to that of the NR SL in Equation (6). Yet, the adsorbed molecules' density can be unequal over the nanoribbons and in the gaps between them. Two extreme alternatives are:

Model 1 - Molecules distributed evenly over the whole interface

In this model, we will assume that the molecules are adsorbed to the whole interface, not only to the graphene nanoribbons. The conductivities, $\sigma_1(\omega)$ and $\sigma_2(\omega)$, are given by

$$\begin{cases} \sigma_1(\omega) = \sigma_G(\omega) + \sigma_M(\omega) \\ \sigma_2(\omega) = \sigma_M(\omega) \end{cases} . \tag{41}$$

Model 2 - Molecules adsorbed only by the NRs

In this model, we will consider a system composed of parallel graphene strips with molecules stuck to them, intercalated by clean SiO_2 surface. Then we have:

$$\begin{cases} \sigma_1(\omega) = \sigma_G(\omega) + \sigma_M(\omega) \\ \sigma_2(\omega) = 0 \end{cases} . \tag{42}$$

In order to compare calculated results obtained with these two models, we shall keep the total number of molecules the same for both, i.e. the coverage, Θ, will be taken (D/d_1) times larger for the second model.

3 Results

3.1 Simulation of the results obtained by Rodrigo *et al.* [1]

These experimental results have been simulated in the article [1] using a Finite Elements Method (Ansys HFSS software). It requires considering both the graphene and the condensed molecular phase as finite thickness slabs and this is not very convenient because it requires using an effective thickness of graphene, which is not a well-defined quantity. [5] We shall apply our theoretical model described in section 2 to the data of Rodrigo *et al.* [1] using the set of parameters presented on Table 1. Notice that a different value of the dielectric constant of SiO_2 was used here as compared to Figure 1 because we are interested in a different spectral range, which is separated from the low-frequency region by bands of polar optical phonons. [31]
The results will be compared in terms of the extinction coefficient,

$$\text{Extinction} = 1 - \frac{T}{T_0} , \tag{43}$$

where T_0 is the transmittance of the structure without graphene NRs and the molecules, that we calculate by applying Equation (31) with $\sigma_1 = \sigma_2 = 0$. The obtained results are summarized in Figure 2 where we compare the experimental results with our simulations for the two models proposed in the previous section. Notice that the experimental spectra are shifted in the vertical direction in order to facilitate the visualization of the results for different values of the Fermi level, so we did the same in our calculated results.

Table 1: Parameters used in the simulations

Physical quantity	Value	Physical quantity	Value
Damping parameter, Γ	43.9 meV	Air permittivity, ϵ_1	1
Supperlattice period, D	80 nm [1]	SiO_2 permittivity, ϵ_2	1.4 [31]
Width of the first stripe, d_1	30 nm [1]	Width of the second stripe, d_2	50 nm [1]
SiO_2 thickness, d	280 nm	Si permittivity, ϵ_3	11.9
Molecular layer thickness, δ	4 nm [1]	Coverage factor, Θ	1 or 2.7
Vibrational mode 1, ω_1	207 meV [1]	Vibrational mode 2, ω_2	190 meV [1]
Damping parameter 1, γ_1	9.68 meV [1]	Damping parameter 2, γ_2	12.5 meV [1]
Oscillator strength 1, S_1	26.4 meV [1]	Oscillator strength 2, S_2	24.8 meV [1]

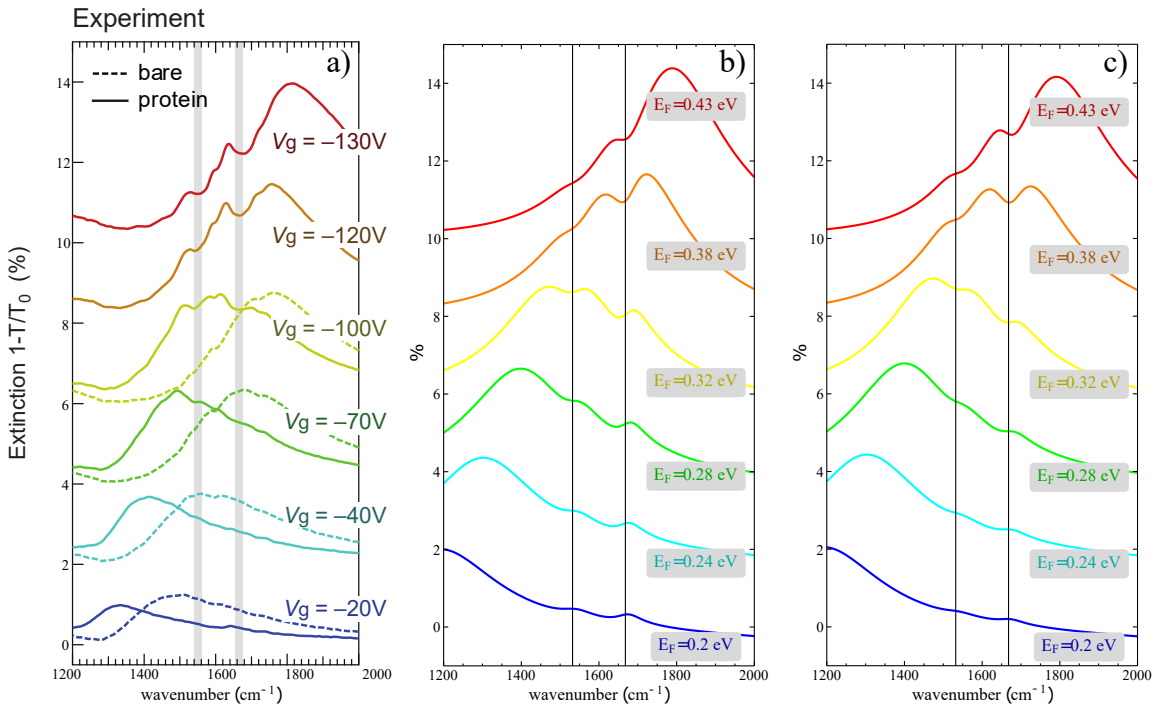

Figure 2: (a) Experimental results by Rodrigo *et al.* [1] and our calculated extinction spectra obtained for: (b) Model 1 – Molecules over the whole interface, and (c) Model 2 – Molecules only over the nanoribbons.

Our calculated results are in excellent agreement with the experimental data, at least as good as in Ref. [1] Somewhat counter-intuitive, Model 1 (with molecules covering evenly the whole interface) seems to reproduce the experimental results slightly better. We also notice that the coverage used by us for this model, $\Theta = 1$, is smaller than the corresponding quantity used by Rodrigo *et al.* in their simulations, which considered a bilayer of protein molecules with the thickness $2\delta = 8$ nm.

3.2 Application to an OMC molecule

Sensors based on this principle should work for any molecules that have IR-active vibrational modes. Let us consider another potentially interesting example, the OMC molecule $Cd(CH_3)_2$. This compound is important, for instance, in the technologies of CdTe growth in the forms of epilayers [32] and nanocrystals (quantum dots). [33]

The molecule is schematically shown in in Figure 3. It is linear and symmetric with respect to the Cd atoms and the Cd-C bonds are polar, with the equilibrium length of 0.213 nm. [34] It possesses two vibrational modes due to the stretching/compression of these bonds, of which only the asymmetric one is IR active, with the frequency $\omega_{AS} = 534cm^{-1}$. [35] This frequency falls into the region where the dielectric function of SiO_2 varies strongly because of the optical phonon resonances. [31] Although coupling of the phonons to the graphene plasmons can be interesting by itself, [36] it would certainly complicate interpretation of the spectra aimed at the molecular sensing. Therefore, we shall assume that graphene NRs are deposited directly on silicon; the necessary FET-type structure may be achieved by using an intrinsic Si layer on top of n-Si.

Apart from this, we apply the same procedure as before, i.e. we derive the 2D conductivity of the molecular layer, Equation (37) in terms of the $Cd(CH_3)_2$ polarisability owing to the IR-active vibration mode,

$$\alpha_0(\omega) = \frac{A}{\omega_{\rm AS}^2 - \omega^2 - i\omega\gamma}\ , \tag{44}$$

and add it to the graphene conductivity according to our Models 1 and 2. As shown in the SI, the amplitude A can be expressed in terms of the atomic masses and the effective charge q (Figure 3) as fol-

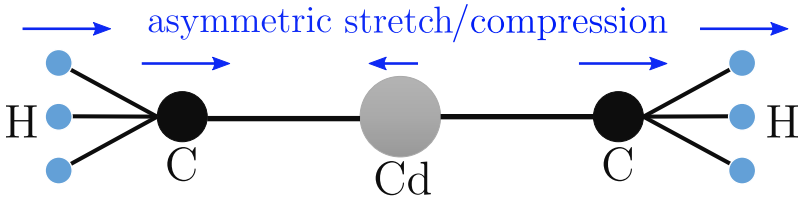

Figure 3: Diagram of the $Cd(CH_3)_2$ molecule. The arrows represent the asymmetric vibrational mode of the molecule.

lows:

$$A = 2q^2 \frac{2m + M}{mM}, \tag{45}$$

where M and m are the masses of the Cd atom and the CH_3 fragment, respectively. The NR SL parameters need to be adjusted in such a way that its first surface plasmon resonance (shown in Figure 1) falls in the vicinity of ω_{AS}. The following approximate formula [37] for the resonance frequency is helpful for this:

$$\omega_R = \frac{4}{D}\sqrt{\frac{\pi\alpha_f c}{\hbar}\frac{d_1 E_F}{\epsilon_1 + \epsilon_2}}, \tag{46}$$

where α_f is the fine structure constant and d_1 is the NR width.
Figure 4 shows the extinction spectra calculated for the two models of their adhesion to the structure. In both cases, one can easily see the presence of a sharp feature corresponding to the vibrational mode of the OMC molecule superimposed onto a broad plasmon resonance band. The feature is more clearly seen in the case of molecules stuck only to the NRs (remind that we used $\Theta = 2$ right panel in Figure 4, while $\Theta = 1$ for the Model 1). The height of the peak, for the lowest values of the Fermi energy, coincides with that characteristic of the molecular layer if deposited on the substrate without graphene NRs. Interestingly, the shape of the $Cd(CH_3)_2$ related feature changes from a peak to a dip when it passes from the wing to the middle of the plasmonic band with the increase Fermi energy. This shape clearly

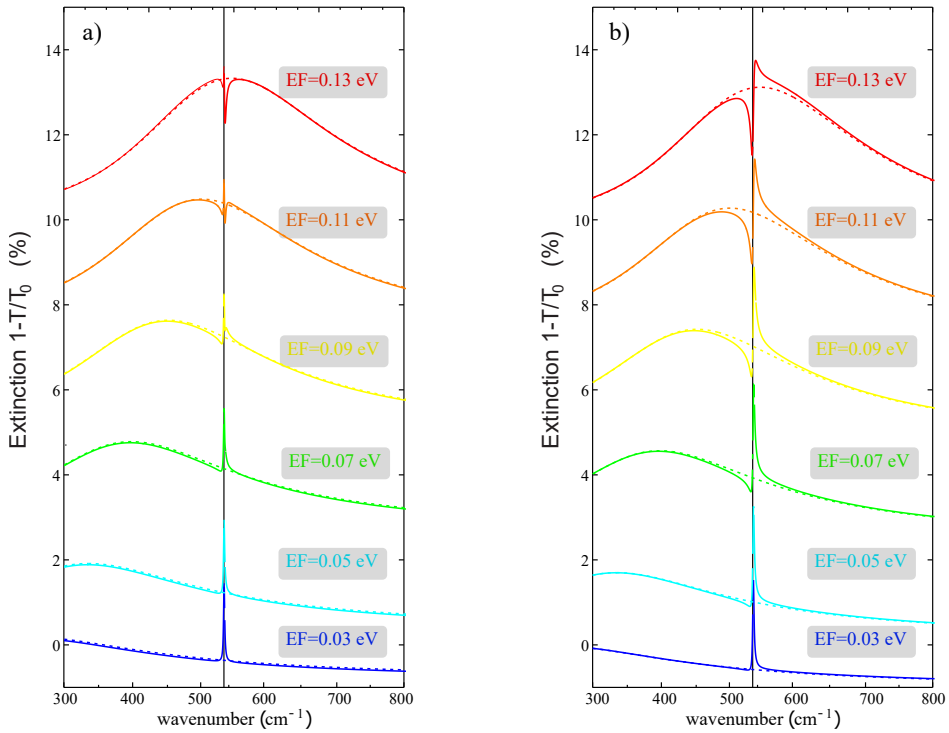

Figure 4: Calculated extinction spectra for $Cd(CH_3)_2$ for graphene NR SL on a Si substrate: (a) Model 1 – Molecules over the whole interface, (b) Model 2 – Molecules only over the NRs. Parameters: $N_M^{(2D)} = 7 \times 10^{14}$ cm^{-2} [34], $\omega_{AS} = 534$ cm^{-1}, $\gamma = 2$ cm^{-1}, $D = 40$ nm, $d_1 = d_2 = 20$ nm, and $q = e$. The dashed lines are the extinction spectra without OMC molecules.

is of the Fano type for $E_F \geq 0.07$ eV. Indeed, here we have a superposition of the narrow molecular resonance and the broad plasmonic band, a condition for the Fano resonance. [38]

4 Conclusion

We have shown that the theoretical model presented here, based on a semi-analytical approach and treating the graphene NR superlattice and the layer of adsorbed molecules as two-dimensional, reproduces very well the experimental data of Rodrigo *et al.* [1] who first implemented this type of sensor. Our model has the advantage of requiring lower computational resources as compared to Maxwell equations' solvers based numerical methods such as the Finite elements one. Moreover, it allows one to try different models of adsorption of analyte molecules to the sensor surface. The thickness of the buffer layer between the NR SL and the (silicon) substrate was shown to influence the signal via interference between the incident waves (for each scattering order n, i.e. for in-plane wavevector $(k_x + 2n\pi/D)$) and those reflected from the buffer/substrate interface (Figure 1).
We also applied it to another potentially interesting example, namely, the $Cd(CH_3)_2$ molecules. Although we obtained a clearly detectable feature in the extinction spectra of the sensor structure in this case, a word of caution is necessary in this respect. Since the effective charge involved in the polar Cd-C bond is not known, we took it as equal to the electron charge, which is probably an exaggeration. With this charge and the bond length of 0.213 nm we obtain a static dipole moment of 10.2 D, while the dipole moments of the most common molecular bonds are just of the order of 0.5 - 3.5 D. [39] Of course, the dynamic charge revealing itself in the vibrations is not the same as the static one in polar molecules, still, the amplitude of the calculated $Cd(CH_3)_2$ signal may be overestimated. It means than the detection would require not just one but few monolayers of adsorbed molecules. In this respect, the modelled type of sensor can hardly compete with the molecular detection based on SERS, [22,40] which, however, has its own drawbacks.

Supporting Information
Supporting Information is available from the Wiley Online Library or from the author.

Conflict of Interest
The authors declare no conflict of interest.

Acknowledgements
Funding from the Portuguese Foundation for Science and Technology (FCT) in the framework of the Strategic Financing UID/FIS/04650/2019. Authors also acknowledge FEDER and the Portuguese Foundation for Science and Technology (FCT) for support through projects POCI-01-0145-FEDER-028114 and PTDC/FIS-MAC/28887/2017. MIV also acknowledges support from the European Commission through the project "Graphene-Driven Revolutions in ICT and Beyond"- Core 3 (Ref. No. 881603).

References

[1] D. Rodrigo, O. Limaj, D. Janner, D. Etezadi, F. G. de Abajo, V. Pruneri, H. Altug, *Science* **2015**, *349* 165.

[2] A. C. Ferrari, F. Bonaccorso, V. Fal'ko, K. S. Novoselov, S. Roche, P. Bøggild, S. Borini, F. H. L. Koppens, V. Palermo, N. Pugno, J. A. Garrido, R. Sordan, A. Bianco, L. Ballerini, M. Prato, E. Lidorikis, J. Kivioja, C. Marinelli, T. Ryhänen, A. Morpurgo, J. N. Coleman, V. Nicolosi, L. Colombo, A. Fert, M. Garcia-Hernandez, A. Bachtold, G. F. Schneider, F. Guinea, C. Dekker, M. Barbone, Z. Sun, C. Galiotis, A. N. Grigorenko, G. Konstantatos, A. Kis, M. Katsnelson, L. Vandersypen, A. Loiseau, V. Morandi, D. Neumaier, E. Treossi, V. Pellegrini, M. Polini, A. Tredicucci, G. M. Williams, B. Hee Hong, J.-H. Ahn, J. Min Kim, H. Zirath, B. J. van Wees, H. van der Zant, L. Occhipinti, A. Di Matteo, I. A. Kinloch, T. Seyller, E. Quesnel, X. Feng,

K. Teo, N. Rupesinghe, P. Hakonen, S. R. T. Neil, Q. Tannock, T. Löfwander, J. Kinaret, *Nanoscale* **2015**, *7* 4598.

[3] A. Grigorenko, M. Polini, K. Novoselov, *Nat. Photonics* **2012**, *6* 749.

[4] F. G. de Abajo, *ACS Photonics* **2014**, *1* 135–152.

[5] P. A. D. Gonçalves, N. M. R. Peres, *An Introduction to Graphene Plasmonics*, World Scientific, **2016**.

[6] Z. Fei, A. S. Rodin, G. O. Andreev, W. Bao, A. S. McLeod, M. Wagner, L. M. Zhang, Z. Zhao, M. Thiemens, G. Dominguez, M. M. Fogler, A. H. C. Neto, C. N. Lau, F. Keilmann, D. N. Basov, *Nature* **2012**, *487* 82.

[7] J. Chen, M. Badioli, P. Alonso-González, S. Thongrattanasiri, F. Huth, J. Osmond, M. Spasenović, A. Centeno, A. Pesquera, P. Godignon, A. Z. Elorza, N. Camara, F. J. García de Abajo, R. Hillenbrand, F. H. L. Koppens, *Nature* **2012**, *487*, 7405 77.

[8] X. Luo, T. Qiu, W. Lu, Z. Ni, *Materials Science and Engineering: R: Reports* **2013**, *74*, 11 351.

[9] Y. V. Bludov, A. Ferreira, N. M. R. Peres, M. I. Vasilevskiy, *Int. J. Mod. Phys. B* **2013**, *27* 134100.

[10] S. Ogawa, S. Fukushima, M. Shimatani, *Sensors* **2020**, *20* 3563.

[11] A. Woessner, M. B. Lundeberg, Y. Gao, A. Principi, P. Alonso-González, M. Carrega, K. Watanabe, T. Taniguchi, G. Vignale, M. Polini, J. Hone, R. Hillenbrand, F. H. L. Koppens, *Nat. Mater* **2015**, *14* 421.

[12] G. X. Ni, A. S. McLeod, Z. Sun, L. Wang, L. Xiong, K. W. Post, S. S. Sunku, B. Y. Jiang, J. Hone, C. R. Dean, M. M. Fogler, D. N. Basov, *Nature* **2018**, *557* 530.

[13] L. Novotny, B. Hecht, *Principles of Nano-Optics*, Cambridge University Press, **2006**.

[14] L. Ju, B. Geng, J. Horng, C. Girit, M. Martin, Z. Hao, H. A. Bechtel, X. Liang, A. Zettl, Y. R. Shen, F. Wang, *Nat. Nanotechnol.* **2011**, *6* 630.

[15] S. Thongrattanasiri, F. H. L. Koppens, F. J. García de Abajo, *Phys. Rev. Lett.* **2012**, *108* 047401.

[16] A. Y. Nikitin, F. Guinea, F. J. Garcia-Vidal, L. Martin-Moreno, *Phys. Rev. B* **2012**, *85* 081405.

[17] P. Gonçalves, E. Dias, Y. V. Bludov, N. M. R. Peres, *Phys. Rev. B* **2016**, *94* 195421.

[18] V. W. Brar, M. S.Jang, M. Sherrott, J. J. Lopez, H. A. Atwater, *Nano Lett.* **2013**, *13* 2541.

[19] Z. Fang, S. Thongrattanasiri, A. Schlather, Z. Liu, L. Ma, P. M. A. Y. Wang, P. Nordlander, N. J. Halas, F. J. G. de Abajo, *ACS Nano* **2013**, *7* 2388.

[20] C. Lee, B. Lawrie, R. Pooser, K.-G. Lee, C. Rockstuhl, M. Tame, *Chemical Reviews* **2021**, *121* 4743.

[21] F. Wu, P. A. Thomas, V. G. Kravets, H. O. Arola, M. Soikkeli, K. Iljin, G. Kim, M. Kim, H. S. Shin, D. V. Andreeva, C. Neumann, M. Küllmer, A. Turchanin, D. De Fazio, O. Balci, V. Babenko, B. Luo, I. Goykhman, S. Hofmann, A. C. Ferrari, K. S. Novoselov, A. N. Grigorenko, *Scientific Reports* **2019**, *9* 20286.

[22] Q. Hong, J. Luo, C. Wen, J. Zhang, Z. Zhu, S. Qin, X. Yuan, *Opt. Express* **2019**, *27*, 24 35914.

[23] Y. V. Bludov, N. M. R. Peres, M. I. Vasilevskiy, *Phys. Rev. B* **2020**, *101* 075415.

[24] P. R. Griffiths, J. A. D. Haseth, *Fourier transform infrared spectrometry*, John Wiley & Sons, **2007**.

[25] F. Neubrech, A. Pucci, T. W. Cornelius, S. Karim, A. García-Etxarrand, J. Aizpurua, *Phys. Rev.* **2008**, *101* 157403.

[26] R. Adato, H. Altug, *Nature Communications* **2013**, *4* 2154.

[27] B. Ng, S. M. Hanham, J. Wu, A. I. Fernández-Domínguez, N. Klein, Y. F. Liew, M. B. H. Breese, M. Hong, S. A. Maier, *ACS Photonics* **2014**, *1*, 10 1059.

[28] Y. Zhong, S. D. Malagari, T. Hamilton, D. Wasserman, *J. Nanophotonics* **2015**, *9* 93791.

[29] K. Xu, R. Zhou, K. Takei, M. Hong, *Adv. Sci.* **2019**, *6* 1900925.

[30] H. Hu, X. Yang, F. Zhai, D. Hu, R. Liu, K. Liu, Z. Sun, Q. Dai, *Nat.Commun.* **2016**, *7* 1.

[31] R. Kitamura, L. Pilon, M. Jonasz, *Appl. Opt.* **2007**, *46* 8118.

[32] S. N. Ershov, M. I. Vasilevskiy, T. I. Benushis, B. V. Gurilev, A. B. Ozerov, *Semiconductor Science and Technology* **1992**, *7*, 2 245.

[33] A. L. Rogach, editor, *Semiconductor Nanocrystal Quantum Dots*, Springer-Verlag, Wien, **2008**.

[34] F. Hanke, S. Hindley, A. C. Jones, A. Steiner, *Chem. Commun.* **2016**, *52* 0144–10146.

[35] J. R. Durig, S. C. Brown, *J. Mol. Spectrosc.* **1973**, *45* 338.

[36] M. Badioli, A. Woessner, K. J. Tielrooij, S. Nanot, G. Navickaite, T. Stauber, F. J. García de Abajo, F. H. L. Koppens, *Nano Letters* **2014**, *14*, 11 6374, pMID: 25343323.

[37] C. Sorger, S. Preu, J. Schmidt, S. Winnerl, Y. V. Bludov, N. M. R. Peres, M. I. Vasilevskiy, H. B. Weber, *New Journal of Physics* **2015**, *17*, 5 053045.

[38] U. Fano, *Phys. Rev.* **1961**, *124* 1866.

[39] R. J. Quellette, J. D. Rawn, *Principles of Organic Chemistry*, Elsevier, **2015**.

[40] H. Lai, F. Xu, Y. Zhang, L. Wang, *J. Mater. Chem. B* **2018**, *6* 4008.

Table of Contents

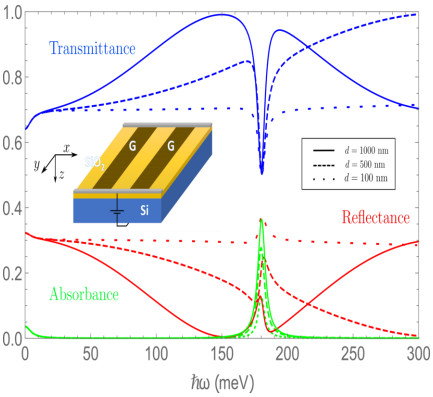

ToC Entry

We present a semi-analytical theoretical model, which describes the operation of a selective molecular sensor employing a double resonance between a dipole-active molecular vibration mode, tunable surface plasmons in a periodic structure of graphene nanoribbons (NRs), and the incident light, in the THz-to-IR range. The model is applied to two different molecular systems, the A/G-IgG protein and an organometallic compound.